Cell Reports

The interplay between metabolic stochasticity and cAMP-CRP regulation in single *E. coli* cells

Graphical abstract

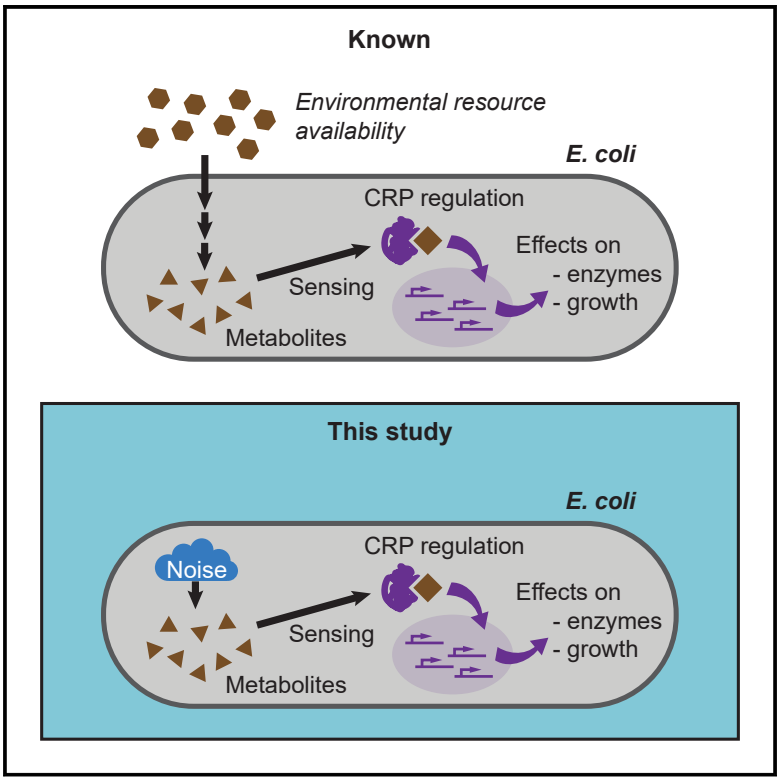

Highlights

- Single-cell experiments show noise regulation by cAMP-CRP system
- Bacteria respond to internal metabolic noise, not just external nutrient changes
- Enzyme expression is continuously adjusted to internal metabolic fluctuations
- Modeling predicts metabolic noise reverberations throughout the cell

Authors

Martijn Wehrens, Laurens H.J. Krah, Benjamin D. Towbin, Rutger Hermsen, Sander J. Tans

Correspondence

tans@amolf.nl

In brief

Wehrens et al. track single *E. coli* cells to show that they continuously respond to internal stochastic fluctuations in metabolite concentrations, hence showing a function of the CRP master regulator beyond adjusting to external conditions. The findings suggest that many metabolic regulation mechanisms act to achieve metabolic homeostasis in constant external conditions.

Wehrens et al., 2023, Cell Reports *42*, 113284
October 31, 2023
https://doi.org/10.1016/j.celrep.2023.113284

CellPress

Cell Reports

CellPress
OPEN ACCESS

Report

The interplay between metabolic stochasticity and cAMP-CRP regulation in single *E. coli* cells

Martijn Wehrens,[1,2,8] Laurens H.J. Krah,[3,4,8] Benjamin D. Towbin,[5] Rutger Hermsen,[3,4,7] and Sander J. Tans[1,6,7,9,*]
[1]AMOLF, 1098 XG Amsterdam, the Netherlands
[2]Hubrecht Institute, Royal Netherlands Academy of Arts and Sciences (KNAW) and University Medical Center, 3584 CT Utrecht, the Netherlands
[3]Theoretical Biology Group, Biology Department, Utrecht University, 3584 CH Utrecht, the Netherlands
[4]Centre for Complex Systems Studies, Utrecht University, 3584 CE Utrecht, the Netherlands
[5]Institute of Cell Biology, University of Bern, 3012 Bern, Switzerland
[6]Department of Bionanoscience, Kavli Institute of Nanoscience, Delft University of Technology, 2629 HZ Delft, the Netherlands
[7]Senior author
[8]These authors contributed equally
[9]Lead contact
*Correspondence: tans@amolf.nl
https://doi.org/10.1016/j.celrep.2023.113284

SUMMARY

The inherent stochasticity of metabolism raises a critical question for understanding homeostasis: are cellular processes regulated in response to internal fluctuations? Here, we show that, in *E. coli* cells under constant external conditions, catabolic enzyme expression continuously responds to metabolic fluctuations. The underlying regulatory feedback is enabled by the cyclic AMP (cAMP) and cAMP receptor protein (CRP) system, which controls catabolic enzyme expression based on metabolite concentrations. Using single-cell microscopy, genetic constructs in which this feedback is disabled, and mathematical modeling, we show how fluctuations circulate through the metabolic and genetic network at sub-cell-cycle timescales. Modeling identifies four noise propagation modes, including one specific to CRP regulation. Together, these modes correctly predict noise circulation at perturbed cAMP levels. The cAMP-CRP system may thus have evolved to control internal metabolic fluctuations in addition to external growth conditions. We conjecture that second messengers may more broadly function to achieve cellular homeostasis.

INTRODUCTION

Bacteria display a striking ability to adapt to diverse environments. When exposed to different carbon sources, bacterial cells make vast changes to their proteome composition, allowing them to optimize their allocation of metabolic resources.[1–4] Many regulation mechanisms have been identified that adjust enzyme expression to the growth medium.[5–8] In addition to these external changes, however, bacteria are also confronted with major internal variations, even under constant external conditions.[9,10] Gene expression has long been known to be stochastic.[9–12] More recently, the metabolic activity of cells was also found to fluctuate randomly, severely limiting growth.[13–17] These findings raise the question of whether cells employ regulatory mechanisms to adjust the proteome in response to stochastic internal metabolic fluctuations.

Studying this issue is non-trivial. Cellular changes caused by external nutrients or internal stochasticity are notably different, even as most specifics are poorly understood. For instance, the former are transmitted by specific pathways and components, lead to sustained growth and expression capacity changes, and occur typically on longer timescales.[18–21] In contrast, stochastic internal changes are a manifestation of general fluctuations in many components and pathways,[22,23] which are correlated in complex ways,[9,13,24,25] are bound by constant growth and expression capacity over time, and occur on faster timescales.[13,26,27] Whether such metabolic fluctuations are filtered or averaged out, by mechanisms like the competition for limited expression or growth capacity or the secretion of excess metabolites,[28,29] or whether cells continuously respond to them, for instance by modulating expression levels, remains poorly understood. Addressing this issue is key to understanding the elementary principles of cellular homeostasis and the functional relevance of known regulatory interactions.

Here, we address this question using cyclic AMP (cAMP)-cAMP receptor protein (CRP) signaling in *Escherichia coli* as a model system. cAMP-CRP signaling is a major regulation mechanism of metabolic activity (Figure 1A). Regulating over 180 genes, CRP is a general expression activator of a group of catabolic enzymes that together are referred to as the C-sector.[4,19,30,31] CRP is activated by the second messenger cAMP, whose synthesis is in turn inhibited by metabolites that are produced by the C-sector enzymes. The resulting negative feedback loop has been shown to produce a near-linear relation

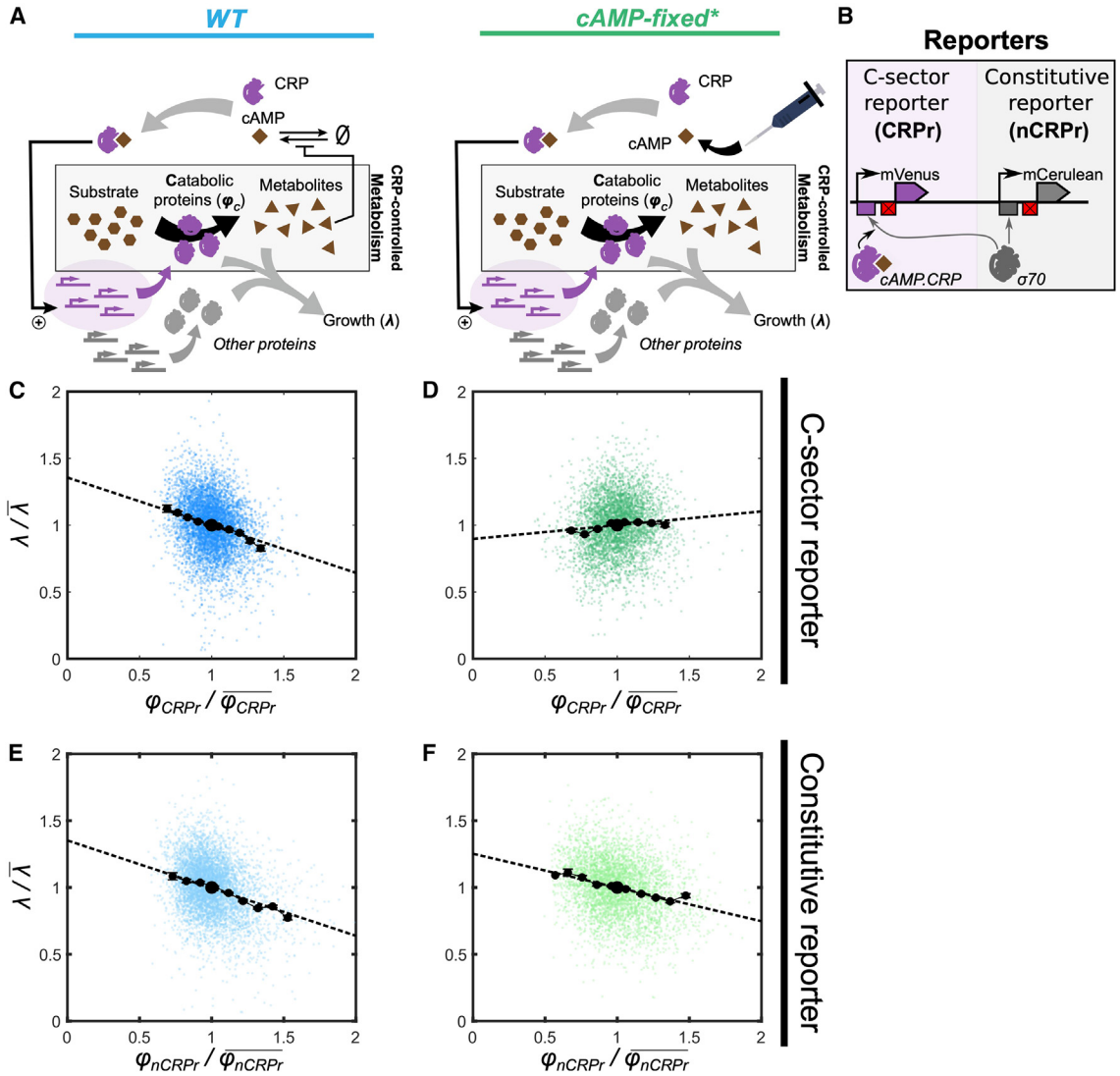

Figure 1. Removing cAMP feedback alters dynamics of a regulated reporter only

(A) Cartoon of a bacterial cell and the difference between WT and mutant. Shown are the processes of metabolism, protein expression, cAMP-CRP regulation, and growth (λ). Here, φ_C represents the expression level of the C-sector, the total concentration of all catabolic proteins that are regulated by cAMP-CRP and that import nutrients and convert them into internal metabolites (including cAMP itself). In the cAMP-fixed strain, cAMP is neither synthesized nor degraded and is instead supplied externally to experimentally tune φ_C.

(B) The two reporters and their promoters that were used in this study: a C-sector reporter whose transcription was regulated by cAMP-CRP (CRPr), and a constitutive reporter, nCRPr. Crossed red block is the scrambled LacI site.

(C–F) Scatterplot of instantaneous growth rate (λ) against single-cell relative expression of the reporters (φ_{CRPr} or φ_{nCRPr}). Dashed lines are linear regressions, and black dots indicate binned averages (± standard error of the mean). Plots are from single, representative microcolonies (n = 1,671 cells for WT, n = 1,580 cells for cAMP-fixed*), and other colonies showed the same trends (Figure S1E).

See also Figure S1 and Table S1.

between the C-sector proteome mass fraction (φ_C) and the growth rate (λ) under variation of the carbon source available in the medium[3,19] and to optimally balance the costs and benefits of C-sector expression such that the overall growth rate is maximized in a range of nutrient conditions.[5] However, the interplay between internal stochastic variations in metabolic activity and the cAMP-CRP system has not been addressed experimentally nor for other metabolic regulatory feedback mechanisms. Note that we lack general information about the metabolic fluctuations that are relevant here: which components and pathways are affected, how these fluctuations correlate and interact, and whether protein expression or growth changes are involved. In contrast to external nutrient changes as studied in steady-state bulk experiments, it is also unclear whether the internal stochastic changes are associated with a specific limitation, such as the availability of carbon or nitrogen. These exigencies, as well as the inherently single-cell nature of the problem, require a different experimental approach.

To study stochasticity in the cAMP-CRP system, we quantified the correlations between C-sector expression and growth rate in individual cells over time using time-lapse microscopy, which allows identification of time delays in the propagation of fluctuating signals. To dissect the role of the cAMP-CRP feedback, we aimed to specifically disrupt its transmission of noise. The challenge here was to maintain the C-sector stimulation by cAMP, which is essential to growth, while eliminating the feedback of cAMP noise. To achieve this, we used an *E. coli cyaA cpdA* null mutant that is unable to synthesize or hydrolyze cAMP.[5] The noise feedback was thus broken, while externally supplied cAMP maintained C-sector expression at appropriate levels (Figure 1A).

In wild-type (WT) cells, C-sector expression showed fluctuations that were negatively correlated and time delayed with respect to growth fluctuations, in line with cAMP-CRP regulating the C-sector in response to metabolic stochasticity. Consistently, disrupting the cAMP-CRP feedback abolished these negative correlations. A mathematical model we developed could explain all the observed correlations in a single fitting procedure, reproducing the observed effect of the disrupted feedback by merely changing the feedback transfer parameter to zero. This mechanistic understanding of the system was further evidenced by the ability of the model to predict the changes in stochastic dynamics for cAMP levels below and above WT levels. Together, the findings show that C-sector expression in *E. coli* is continuously regulated in response to internal stochastic metabolic fluctuations in fixed environments. They also suggest that feedbacks in metabolic networks, which are ubiquitous in cells, act more generally to control and exploit internal metabolic noise.

RESULTS

Interrupting the feedback of noise in the cAMP-CRP system

Elucidating noise propagation in the cAMP-CRP system requires insight into the stochasticity of the C-sector expression that is regulated by CRP. The population-mean C-sector expression was previously studied by quantifying the expression of a representative enzyme, LacZ.[19] Here, we follow this general approach and measure the expression of mVenus driven by the *lac* promotor (Figures 1B and S1A). As we aim to study fluctuations propagated by CRP rather than by the *lac* repressor LacI, the LacI binding site in the lac promotor is scrambled such that LacI no longer binds, while the promotor remains sensitive to cAMP-CRP.[5,32–34] This genome-inserted construct is called the CRP-regulated reporter (CRPr). To study noise unrelated to CRP or LacI, a second reporter was created by further modifying the CRPr promoter. Specifically, the region where CRP and σ^{70} bind was replaced with a σ^{70} consensus site, such that transcriptional initiation occurs constitutively without requiring CRP to recruit σ^{70}. This reporter construct, which was fused to mCerulean, is referred to as the non-CRPr (nCRPr) (Figures 1B and S1A). Both CRPr and nCRPr were chromosomally inserted into *E. coli*, a construct we refer to as WT, and into a *cyaA cpdA* null mutant, which we refer to as cAMP-fixed.

Bulk measurements in lactose minimal media showed that the growth rate of cAMP-fixed peaked at about 800 μM externally supplied cAMP while decreasing to almost negligible growth at lower and higher cAMP concentrations[5,35] (Figure S1B). This strong dependence on cAMP is consistent with the many genes controlled by CRP and their essential nature. At low cAMP, under-stimulation of C-sector expression leads to decreased metabolic flux and concomitant growth. Conversely, at high cAMP, over-stimulation of C-sector expression leads to excess expression of many genes, which is metabolically costly and hence also reduces the growth rate. We find that the growth rate of WT cells in the same lactose minimal medium (without externally supplied cAMP) is similar to the optimal growth rate of cAMP-fixed cells obtained at 800 μM cAMP (Figure S1C). We refer to cAMP-fixed cells growing at 800 μM cAMP as cAMP-fixed* cells. Both WT and cAMP-fixed* cells were also observed as growing microcolonies with phase-contrast and fluorescence time-lapse microscopy. The mean fluorescence intensity per unit area for CRPr and nCRPr was similar for WT and cAMP-fixed* cells (Figure S1D). Overall, these experiments show that WT and cAMP-fixed* cells display comparable population-mean C-sector stimulation and growth rate, allowing us to study whether the propagation of noise in single cells differs between the WT and cAMP-fixed* cells.

The cAMP-CRP system responds to internal stochastic fluctuations

The propagation of and response to cellular noise can be studied by quantifying correlations between fluctuating phenotypic parameters.[13,24,25] Here, we quantify fluctuations in the instantaneous cellular growth rate, λ, by performing phase-contrast microscopy at a time resolution of 1–1.5 min, noting that multiple time points are used to determine one λ value. Fluctuations in CRPr expression levels, φ_{CRPr}, are quantified by the mVenus fluorescence intensity using concurrent fluorescence microscopy at intervals ranging from 13.5 to 26 min. In WT cells, φ_{CRPr} fluctuations were negatively correlated with λ fluctuations, as is apparent from the negative regression slope in Figure 1C. In cAMP-fixed* cells, a positive correlation was found instead (Figure 1D). The difference is statistically significant ($p = 0.0031$, Student's t test, Figure S1E) and suggests that the negative correlation in WT cells is a consequence of cAMP-CRP signaling, which is eliminated in the cAMP-fixed* cells. The negative correlation is reminiscent of the negative relation between C-sector expression and growth rate known as the C-line.[2,4,19] Note, however, that the C-line characterizes the response of a culture under balanced growth for different available carbon substrate(s), rather than the fluctuations within single cells under fixed conditions, and that bulk assays can also yield a positive relation between the C-sector expression and growth rate, for instance under nitrogen limitation.[19]

To assess whether the φ_{CRPr}-λ correlation changes were due to disruption of CRP regulation, we studied the relationship between λ and the expression levels of the reporter not regulated by CRP, φ_{nCRPr}, as quantified by mCerulean fluorescence intensity. The correlations between φ_{nCRPr} and λ were negative for both the WT and the cAMP-fixed* cells and, indeed, were indistinguishable (Figures 1E, 1F, and S1E; $p = 0.93$, Welch's t test). This similarity is consistent with the above hypothesis, as nCRPr is not regulated by cAMP-CRP in either strain. Thus, the growth correlations of the nCRPr were similar with or without the

cAMP-CRP feedback. Conversely, the growth correlations of the CRPr showed a notable shift when this feedback was disrupted, suggesting that the cAMP-CRP system actively responds to internal fluctuations.

Time-dependent cross-correlations are captured by a mathematical model

To obtain a mechanistic understanding of the observed correlations, we extended the model presented by Kiviet et al.[13] Our aim is not to capture the many known molecular mechanisms of the CRP system but rather to assess whether the phenomenological relations between variables are sufficient to describe our data. The model is based on linear stochastic differential equations (SDEs) that describe the temporal dynamics of protein production rates (π) and concentrations (φ), the growth rate (λ), and a parameter that reflects the metabolic activity to which the CRP system responds (M) (Figure 2A). We explicitly modeled the expression of the C-sector (π_C and φ_C), the C-sector reporter (π_{CRPr} and φ_{CRPr}), and the constitutive reporter (π_{nCRPr} and φ_{nCRPr}). Note that the growth rate λ affects the concentration φ, because volume growth dilutes cellular components, but not the production rate π. With this model, we hypothesize that intrinsic stochasticity in λ, π, and M, as modeled by independent Ornstein-Uhlenbeck noise sources, propagate through the network as defined by the interactions drawn in Figure 2A and as quantified by transfer coefficient T. In particular, it surmises that the cAMP-CRP system propagates internal stochastic fluctuations in M backwards to the expression of the C-sector genes, in proportion with the parameter T_R (Figure 2A, purple interaction and purple box). This transmission involves fluctuations in metabolite abundance, cAMP synthesis and degradation, and CRP-mediated transcriptional activation (Figures 2A and S2A; STAR Methods; Data S1).

The resulting theoretical expressions can be fitted to the experimental data, which also allows one to estimate the transfer coefficients, timescales, and noise amplitudes. Here, we focus on the cross-correlation function R, which quantifies the correlation between two time series after one is shifted by a delay τ and provide insight into how noise is transmitted within cellular networks.[13,24,25,36] For example, if noise in signal A affects a downstream signal B with a fixed time delay, the A-B cross-correlation peaks at a positive τ.

For WT cells, we found that the $\varphi_{CRPr} - \lambda$ correlation function ($R_{\varphi_{CRPr}-\lambda}$) is negative at $\tau = 0$ (Figure 2B), consistent with the negative slope between φ_{CRPr} and λ (Figure 1C). For cAMP-fixed* cells, $R_{\varphi_{CRPr}-\lambda}$ was positive at $\tau = 0$ (Figure 2B), consistent with the positive slope observed in Figure 1D. Several other features also became clear. For example, in WT cells $R_{\varphi_{CRPr}-\lambda}$ and $R_{\varphi_{nCRPr}-\lambda}$ were not only negative in magnitude but also peaked at negative delays ($\tau < 0$) (Figure 2B, right). In addition, both $R_{\varphi_{CRPr}-\lambda}$ and $R_{\pi_{CRPr}-\lambda}$ were higher in cAMP-fixed* than in WT cells (Figure 2B, top right). The cross-correlation functions of the constitutive nCRPr for WT and *cAMP-fixed** cells were overall very similar (Figure 2B, bottom).

We simultaneously fitted all 8 cross-correlation functions of Figure 2B, covering WT and cAMP-fixed* cells, the two reporters CRPr and nCRPr, and the production rate π and concentration φ (Figure 2B). In WT cells, the transfer parameter T_R was constrained to negative values, whereas in *cAMP-fixed** cells, it was set to zero to implement the elimination of the cAMP-CRP feedback (Figure 2A, red cross). All other parameters, including noise transfer parameters, noise amplitudes, and timescales, were constrained to having the same value for each of the 8 cross-correlation curves (see STAR Methods and Data S1). Despite these strict fitting constraints, the model described the data quantitatively. In particular, it reproduced the shift for CRPr, from a negative φ-λ correlation with a negative time delay for WT cells to a nearly flat but slightly positive φ-λ correlation for cAMP-fixed* cells, and the lack of such a change for nCRPr (Figure 2B). Hence, these findings indicate that the cAMP-CRP system actively modulates C-sector expression in response to internal metabolic fluctuations.

cAMP-CRP noise circulation can be decomposed into distinct noise propagation modes

Next, we further analyzed the model to understand the underlying noise propagation mechanisms. As described above, we postulated coupled (stochastic) differential equations that reflect the stochastic and regulatory dynamics of the CRP system and from it derived mathematical expressions for the cross-correlation functions. Inspection of these expressions reveals that they are a sum of four noise modes, which we termed the catabolism, dilution, common, and regulation modes (Figure 2C; STAR Methods; Data S1). Each mode yields cross-correlation functions of a particular shape and exhibits an amplitude that depends on the amplitudes of the noise sources and transmission parameters; together, the modes determine the overall cross-correlation function. The modes describe how emitted noise propagates along particular pathways to two quantities and, hence, correlates them (Figures S2A–S2C). In the catabolism mode, a stochastic increase in the production rate of a metabolic enzyme leads to higher enzyme concentrations sometime later and, subsequently, to a higher growth rate. This mode thus contributes a positive peak at a positive delay time to the π-λ cross-correlation. In the dilution mode, stochastic increases in growth rate lead to increased dilution of all proteins, contributing to the φ-λ correlation a negative contribution with a negative delay. The common mode is the result of fluctuations in general components that directly affect the protein production rate as well as the growth rate. Hence, this mode yields a symmetric π-λ cross-correlation but a negative delay for φ-λ because it takes time for a change in production rate to cause a change in concentration. Lastly, the regulation mode represents noise transferred via the cAMP-CRP system. It shows how stochastic increases in metabolism and growth can transiently limit cAMP-CRP-mediated activation of C-sector expression, yielding a symmetric but negative π-λ cross-correlation, as well as a delayed negative φ-λ cross-correlation.

The mathematical analysis moreover revealed that not all modes are present in each of the cross-correlation functions (Figure 2C, bottom table). Interestingly, just the absence and the presence of noise modes can already help to qualitatively understand the shape of the experimentally measured cross-correlations for each reporter and strain (Figures 2B and 2C). First, the analysis of our model suggests that the cross-correlation for the CRPr contains a catabolism mode, whereas the correlation for

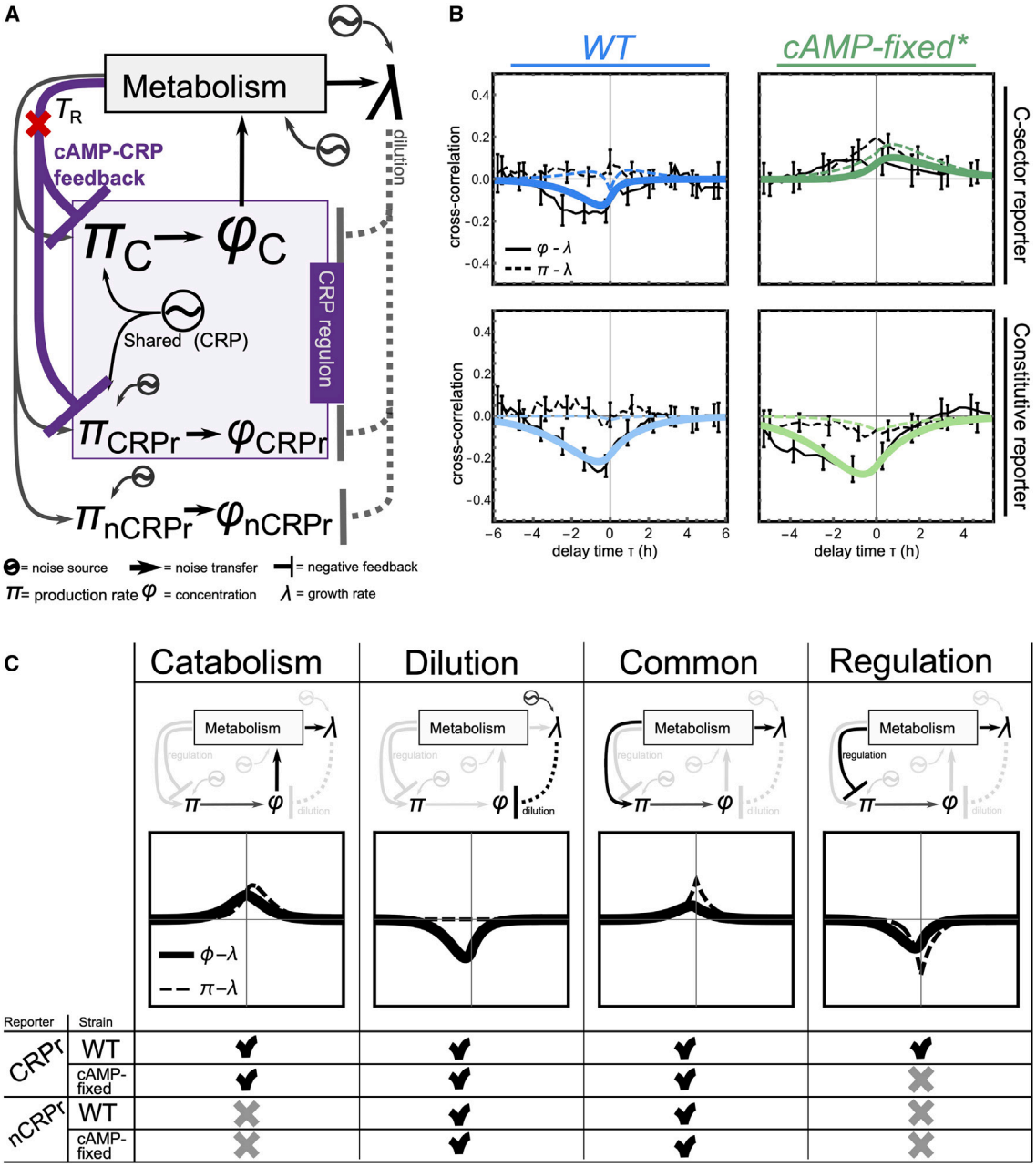

Figure 2. Mathematical model pinpoints dynamical role of regulation

(A) Cartoon of the mathematical model, which considers fluctuations in the growth rate (λ) and the production rates (π) and concentrations (φ) of the C-sector (π_C and φ_C), the C-sector CRPr, and the constitutive nCRPr. Black arrows indicate noise transfer; only fluctuations in φ_C affect metabolism. Metabolism affects growth and protein productions rates. Regulation reacts to metabolic fluctuations and transfers to π_C and π_{CRPr}. In the mutant, regulation is removed (red cross).

(B) Cross-correlation functions between the protein production rate π(t) and λ(t) (dashed lines) and between concentrations φ(t) and λ(t) in the WT and the mutant. Colored lines are model fits, and black lines are cross-correlations calculated from data (6 colonies for WT, with n = 3,635 cells in total, and 4 colonies for cAMP-fixed*, with n = 6,770 cells in total; see Table S1 and Figures S5 and S7), and error bars indicate standard error (see STAR Methods and Data S1, fitting procedure), shown for only some data points.

(C) Interpretation and shape of the underlying noise modes that are present in the model. The checks and crosses indicate whether a mode was included in the model's fit for each experimental condition. The effect of keeping cAMP fixed is reflected by the removal of the regulation mode. Cartoons indicate the direction and route of noise transfer for each specific mode.

See also Figure S2 and Tables S1, and S2.

the nCRPr does not. Note that although neither reporter directly influences the growth rate, the C-sector CRPr can be seen as a proxy for expression of the C-sector, which does influence the growth rate. Therefore, a part of the catabolism mode of the C-sector can be observed in the CRPr cross-correlations but not in the cross-correlations for the constitutive reporter. Second, the regulation mode is only present in the cross-correlations for the C-sector CRPr in the WT because only this reporter is regulated via the cAMP-CRP regulatory network.

We noted that the (cross-)correlations between φ_{CRPr} and λ (Figures 1C and 2B) and between φ_{nCRPr} and λ (Figures 1E and 2B) looked similar in WT cells. The mathematical analysis of the noise propagation model, however, indicates that they are composed of different modes (Figure 2C). For the constitutive nCRPr, in both WT and cAMP-fixed* cells, catabolism and regulation modes are absent, and the main contribution comes from the dilution mode. Cross-correlations of the C-sector reporter CRPr, on the other hand, additionally contain the catabolism and regulation modes, which largely cancel out, resulting in WT correlations with a shape similar to those of nCRPr. In the cAMP-fixed* cells, the negative regulation mode is absent in CRPr correlations, and the catabolism mode becomes visible, resulting in a positive (cross-)correlation.

Given that negative feedback loops can play a role in reducing noise, we wondered whether the cAMP-CRP feedback system could also exert such a functional role. Indeed, a 4% decrease in growth noise and a 7% decrease in C-sector noise in WT compared with the cAMP-fixed* condition are predicted by our model, consistent with a noise-quenching role for the negative feedback (Figures S2D–S2F). The experimentally observed coefficients of variation (CVs) showed a similar trend (Figures S2D and S3E), although such small decreases in growth noise cannot be determined in a statistically significant manner given the levels of measurement noise. Taken together, these observations show that temporal dynamics can be modeled as a linear combination of modes, consistent with the idea that multiple cellular processes, including metabolism and regulation, shape cellular heterogeneity.

Mechanistic model predicts noise propagation for non-optimal C-sector expression

To further test the model, we sought to describe the effects of changes in the population-mean expression of the C-sector. Hence, we examined cAMP-fixed cells with cAMP concentrations below and above the optimal value, here referred to as cAMP-fixed^{low} and cAMP-fixed^{high} cells. Consistently, the measured population-mean expression of the C-sector CRPr was below or above that of *cAMP-fixed** cells, respectively (Figure 3A, black dots). Notably, the constitutive nCRPr showed the opposite: the mean expression was higher in cAMP-fixed^{low} and lower in cAMP-fixed^{high} cells (Figure 3B, red and orange clouds). These observations are consistent with limitations to the size of the overall proteome within cells: when the C-sector becomes larger, the other proteins must decrease in abundance if the total is constrained[2] (Figures S3A and 3C). The slow growth of cAMP-fixed^{low} cells is consistent with the C-sector becoming growth limiting when under-expressed, while the slow growth of cAMP-fixed^{high} cells is in line with the metabolic costs of superfluously over-expressing the C-sector.[5,13,37]

Given these population-mean changes, the model (Figure 2A) yielded several predictions for the stochastic dynamics. In the cAMP-fixed^{low} cells, the growth limitation of the under-expressed C-sector should increase noise transfer from the C-sector enzyme concentration φ_C to metabolism M and on to the growth rate λ and the protein production rate π (Figure 3D, bottom left). The associated increases in the transfer coefficients predict overall increases in the φ-λ and π-λ correlation functions, owing to increased amplitude of the catabolism mode, while the dilution and common modes remain largely unchanged (Figures 2C and S3B). We indeed observed that the CRPr correlations, which were positive for cAMP-fixed* cells, had further increased in magnitude, while the nCRPr correlations became less negative (Figures 3D, S3B, and S3D–S3M). These findings indicate that transient upward fluctuations in C-sector expression can alleviate metabolic bottlenecks caused by mis-regulated C-sector expression, which is on average below the optimum, and hence produce larger increases in growth rate than at optimal C-sector expression.

In the cAMP-fixed^{high} cells, the burden of superfluous C-sector expression implies that it now negatively affects metabolism and growth. The corresponding change from positive to negative values for the transfer parameter from φ_C to M (Figure 2A) predicts φ-λ correlations that are strongly negative (Figure S3C; STAR Methods; Data S1, low and high cAMP), as now only the weaker common mode yields positive correlations, while both the catabolism and dilution modes are negative (Figure 2C). The π-λ correlations are predicted to remain positive, however, as M couples to λ and π, which positively correlates them (Figure 2A). The experiments indeed showed a strongly negative φ-λ correlation (Figure 3E, solid lines), while π-λ correlations are positive or negligible (Figure 3E, dashed lines), in line with these predictions (Figure S3C). More quantitative fits (Figures 3D and 3E) were obtained by increasing the noise amplitudes of the reporters, which decorrelates the signals (see also STAR Methods and Data S1, low and high cAMP). Possibly, such changes in noise amplitudes are caused by changes in average expression levels and mean growth rate, as noise amplitudes tend to increase with the mean.[10,38,39] These experiments indicate that stochastic variations in superfluous expression can cause growth penalties and that our model captures key aspects of the stochastic dynamics.

The data also showed notable distinctions between population-mean and single-cell behaviors: the regression lines through single-cells clouds (Figures 3A and 3B, dashed lines) were typically not tangent to the curves through the population-mean values (Figures 3A and 3B, solid lines, Figure S3A). In some cases even the sign of the single-cell correlations were not consistent with the population-mean trend (Figure 3B, orange cloud). This can be understood as follows. The regression lines describe the integrated response of both variables to internal fluctuations in many cellular components under fixed external conditions. In contrast, the curves describe the response of the mean values of these variables to a specific external perturbation (a change in the externally supplied cAMP concentration). These considerations underscore the difference between internal stochastic variations and external nutrient variations, for instance in terms of growth limitation. It is also of interest to note that the trade-off between C-sector and other proteins,

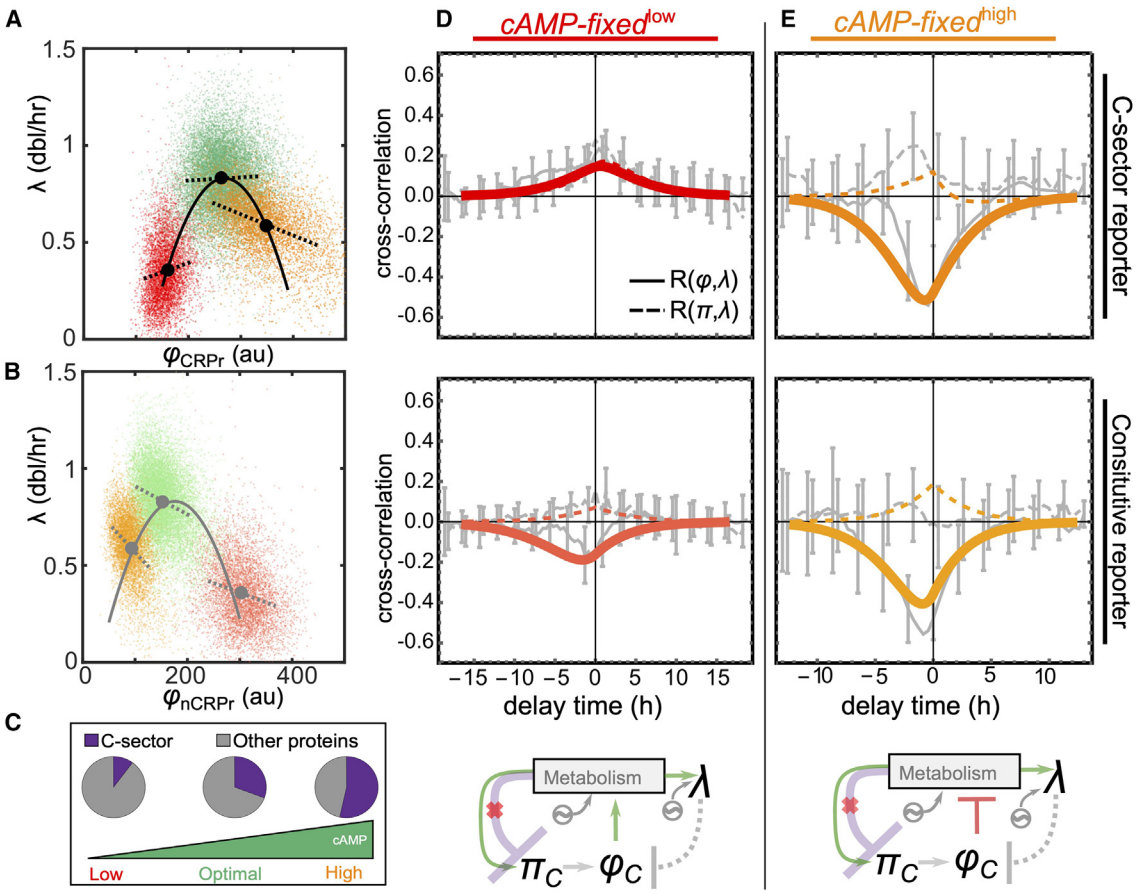

Figure 3. Excessive or insufficient cAMP dampens growth and changes noise-mode amplitudes

(A) Scatterplot of the C-sector reporter against the growth rate under three conditions: low external cAMP (red cloud), optimal cAMP (green cloud, same condition as in Figures 1D and 2B), and high external cAMP (orange cloud). Black dots indicate averages, dashed lines are linear regressions (extending 2 SD to each side), and black curve is a second-order polynomial fit to the means.

(B) Same as in (A) but for the constitutive reporter. Gray parabola is calculated from a sum constraint of both reporters (STAR Methods and Data S1, toy model of the means of the two reporters).

(C) Cartoon showing how increasing the external cAMP concentration increases the size of the C-sector in the mutant strain but represses other proteins.

(D and E) Measured cross-correlations (gray lines with error bars indicate standard error) for both reporters for low cAMP (80 μM) and high cAMP (2,000 μM), together with model predictions (colored lines) resulting from minimal parametric changes compared with the WT fit. Model cartoons (bottom) indicate changes in transfer parameters (green: increase, red: decrease) with respect to cAMP-fixed* cells (see STAR Methods and Data S1, low and high cAMP). Data from two microcolonies are shown for low and high cAMP, with, respectively, n = 1,788 and 2,274 cells in total.

See also Figure S3 and Table S1.

which we here also observe for the population mean (Figure S3A, top left), is not obeyed at the single-cell level at high cAMP, as the correlation between the concentrations of the two reporters in the cAMP-fixed^{high} condition is positive (95% confidence interval [CI] [0.67,0.699]).

DISCUSSION

It has become increasingly clear over the past decade that metabolic networks exhibit stochastic fluctuations.[13,15,17,40] Metabolic networks are also well known to contain numerous regulatory mechanisms that allow cells to react to external changes, which raises the question of whether they also act in response to internal noise. Addressing this question is critical to understanding whether metabolic homeostasis requires continuous regulatory adjustments and to elucidating the functional relevance of known regulatory mechanisms. Here, we studied this issue for the cAMP-CRP metabolic regulation system by experimentally disrupting noise transmission while maintaining the proper population-mean activity. Using single-cell measurements and mathematical modeling, we found that the cAMP-CRP system modulates the expression of the large group of metabolic enzymes called the C-sector in response to stochastic variations within the metabolic network. Our quantitative approach allowed us to reveal the complex noise circulation pathways within the cAMP-CRP system, which can nonetheless be dissected into distinct and additive noise propagation modes. These noise propagation modes describe how catabolic activity, dilution by volume growth, generic metabolic activity,

and cAMP-CRP regulation couple expression and growth in dynamic terms.

Relations between C-sector protein expression and growth have been studied extensively for the case of external nutrient changes.[2,3,19,41] This relation can be negative, for changes in carbon availability, or positive, for changes in nitrogen, ammonium, or sulfate availability, for instance. For the case considered here, it is not *a priori* clear what is limiting, as internal stochastic changes are a manifestation of fluctuations in essentially all cellular components rather than changes in a single external or internal parameter. Fluctuation in multiple internal parameters can also be correlated with each other in a complex and delayed fashion, further obscuring insight. While many details of noise circulation along the many cellular pathways remains an open question, here we show that internal stochastic fluctuations yield a negative correlation between C-sector expression and growth and that the cAMP-CRP feedback is responsible. The "regulation" noise mode in our data, which produces negative C-sector-growth correlations (Figure 2C), is mechanistically closest to what causes the C-line for different carbon sources. However, other noise modes produce positive correlations, which could thus also have resulted in overall positive correlations. Our results also indicate that noise filtering mechanisms, which could potentially have blocked propagation through the pathways studied here, were not dominant. For instance, metabolic and expression fluctuations could have been filtered by limitations in resources including metabolites and ribosomes, excess metabolite secretion, and slowly changing processes such as gene expression and dilution, as well as known and unknown (allosteric) regulation. cAMP-CRP fluctuations and their propagation thus are large and efficient enough to overcome these possible filtering mechanisms.

By showing the interaction between metabolic noise, cAMP-CRP signaling, and noise in the growth rate, this work builds on a growing literature on noise in gene expression in the context of metabolism and growth,[13,25,42–47] as well as earlier, theoretical, work that mainly focused on metabolic noise propagation within particular regulatory networks[48–50] and their influence on expression noise. A common finding is that negative feedback can serve to reduce and control noise amplitudes.[51–53] Consistently, both our model and data show a small decrease (4%–7%) in noise amplitudes when the negative cAMP-CRP feedback is present. Such modest noise differences are difficult to establish experimentally, and indeed, they are not statistically significant here. At the same time, small differences in growth noise could nonetheless be functionally relevant on evolutionary timescales.

While our phenomenological model reproduced the key experimental findings, it is interesting to speculate about relations to additional mechanisms. The C-sector is subject to global regulation, but each gene within it can be affected by intrinsic noise and other gene-specific variations, which contribute to heterogeneity in metabolite concentrations and metabolic fluxes.[17,54,55] Metabolic noise within our model therefore may be viewed as the compound result of the expression and resulting metabolic noise of many enzymes. Metabolic noise is detected by the cAMP-CRP feedback and transmitted backwards to the entire C-sector that drives metabolism. Hence, noise originating in many pathways can reverberate globally through the cell: multiple cellular processes can transmit, modify, and amplify noise such that it becomes difficult to disentangle source from intermediary.

While CRP is an important master regulator, many other secondary messengers and regulatory mechanisms in metabolic networks are known to respond to external growth conditions. For instance, (p)ppGpp is a crucial global modulator of protein expression, cellular growth, ribosome biogenesis, and cell size upon changes in growth media.[56–58] The notion that metabolic regulation mechanisms can also serve to detect and transmit stochastic fluctuations of metabolites, as we show here, may well apply to these and other regulators. Since stochastic fluctuations could occur in any metabolite, including those that exert allosteric control, our findings suggest that noise may propagate through the cellular networks via diverse and complex feedback mechanisms. We surmise that an understanding of the elementary underlying mechanisms is critical to understanding how cells achieve metabolic homeostasis, as well as how they diversify into heterogeneous populations.

Limitations of the study

The C-sector comprises many genes that are central to *E. coli* metabolism. In this study, we focused on the global regulator of this group of genes, using the Lac promoter as reporter construct, following and consistent with previous steady-state studies. However, other regulators that, for instance, act more locally may lead to differences between C-sector genes. While these mechanisms were not modified here and hence would not change the findings, one should be careful in drawing conclusions for specific genes within the C-sector. Another limitation is that our method does not measure fluctuations in metabolites directly but rather is based on correlations between gene expression and growth, mutants that abolish the cAMP-CRP feedback, and mathematical modeling. While methods to measure stochastic fluctuations in the metabolites that are key here are not yet accessible, these may become available in the future.[59] More generally, measurements of gene expression and growth fluctuations are limited by experimental noise. Both are affected by non-perfect focusing, imaging artifacts, and cell segmentation errors, while the former is affected by bleaching and the latter by non-perfect fitting of the size vs. time data. Hence, the method is less suitable for studying absolute measures of expression and growth. As a result, we study here relative measures such as fluctuations and correlations. Our modeling framework addresses the propagation of noise in gene expression and growth around a constant average. It is not suitable to study responses to environmental changes that prompt cells to adjust these average values. Modeling approaches that integrate both noise propagation and changing means in response to changing environments could be used to further understand the differences and interplay between responses to external and internal variations. Such an extension of the model may also allow for a more straightforward interpretation of model parameters. In addition, our model is coarse grained and does not explicitly describe metabolic compounds. While a more detailed model might help to further understand the biological implications of the noise transmission dynamics, the associated increased number of parameters carries fitting and interpretation challenges.

STAR★METHODS

Detailed methods are provided in the online version of this paper and include the following:

- KEY RESOURCES TABLE
- RESOURCE AVAILABILITY
  - Lead contact
  - Materials availability
  - Data and code availability
- EXPERIMENTAL MODEL AND SUBJECT DETAILS
  - Microbe strains
  - Bulk measurements
  - Single cell experiments
- METHOD DETAILS
  - Microscopy
  - Image analysis
  - Mathematical model
- QUANTIFICATION AND STATISTICAL ANALYSIS
  - Cross-correlation analysis

SUPPLEMENTAL INFORMATION

Supplemental information can be found online at https://doi.org/10.1016/j.celrep.2023.113284.

ACKNOWLEDGMENTS

L.H.J.K. was supported by the Dutch Research Council (NWO, www.nwo.nl; grant 022.005.023). This work received funding from the Swiss National Science Foundation (SNSF) in the form of an Eccellenza Professorial Fellowship (PCEFP3_181204) to B.D.T. Work in the group of S.J.T. is supported by the Dutch Research Council (NWO).

AUTHOR CONTRIBUTIONS

Conceptualization, M.W., L.H.J.K., R.H., and S.J.T.; methodology, M.W., L.H.J.K., and B.D.T.; formal analysis, M.W. and L.H.J.K.; investigation, M.W. and L.H.J.K.; resources, B.D.T.; writing – original draft, M.W. and L.H.J.K.; writing – review & editing, B.D.T., R.H., and S.J.T.; visualization, M.W. and L.H.J.K.; supervision, R.H. and S.J.T.; funding acquisition, L.H.J.K., R.H., and S.J.T..

DECLARATION OF INTERESTS

The authors declare no competing interests.

Received: November 21, 2022
Revised: July 17, 2023
Accepted: September 29, 2023

REFERENCES

1. Klumpp, S., and Hwa, T. (2014). Bacterial growth: global effects on gene expression, growth feedback and proteome partition. Curr. Opin. Biotechnol. *28*, 96–102. https://doi.org/10.1016/j.copbio.2014.01.001.
2. Scott, M., Gunderson, C.W., Mateescu, E.M., Zhang, Z., and Hwa, T. (2010). Interdependence of Cell Growth and Gene Expression: Origins and Consequences. Science *330*, 1099–1102. https://doi.org/10.1126/science.1192588.
3. Hui, S., Silverman, J.M., Chen, S.S., Erickson, D.W., Basan, M., Wang, J., Hwa, T., and Williamson, J.R. (2015). Quantitative proteomic analysis reveals a simple strategy of global resource allocation in bacteria. Mol. Syst. Biol. *11*, 784.
4. Schmidt, A., Kochanowski, K., Vedelaar, S., Ahrné, E., Volkmer, B., Callipo, L., Knoops, K., Bauer, M., Aebersold, R., and Heinemann, M. (2016). The quantitative and condition-dependent Escherichia coli proteome. Nat. Biotechnol. *34*, 104–110. https://doi.org/10.1038/nbt.3418.
5. Towbin, B.D., Korem, Y., Bren, A., Doron, S., Sorek, R., and Alon, U. (2017). Optimality and sub-optimality in a bacterial growth law. Nat. Commun. *8*, 14123. https://doi.org/10.1038/ncomms14123.
6. Molenaar, D., van Berlo, R., de Ridder, D., and Teusink, B. (2009). Shifts in growth strategies reflect tradeoffs in cellular economics. Mol. Syst. Biol. *5*, 323. https://doi.org/10.1038/msb.2009.82.
7. Bosdriesz, E., Molenaar, D., Teusink, B., and Bruggeman, F.J. (2015). How fast-growing bacteria robustly tune their ribosome concentration to approximate growth-rate maximization. FEBS J. *282*, 2029–2044. https://doi.org/10.1111/febs.13258.
8. Scott, M., Klumpp, S., Mateescu, E.M., and Hwa, T. (2014). Emergence of robust growth laws from optimal regulation of ribosome synthesis. Mol. Syst. Biol. *10*, 747.
9. Elowitz, M.B., Levine, A.J., Siggia, E.D., and Swain, P.S. (2002). Stochastic gene expression in a single cell. Science *297*, 1183–1186. https://doi.org/10.1126/science.1070919.
10. Taniguchi, Y., Choi, P.J., Li, G.-W., Chen, H., Babu, M., Hearn, J., Emili, A., and Xie, X.S. (2010). Quantifying E. coli proteome and transcriptome with single-molecule sensitivity in single cells. Science *329*, 533–538. https://doi.org/10.1126/science.1188308.
11. Eling, N., Morgan, M.D., and Marioni, J.C. (2019). Challenges in measuring and understanding biological noise. Nat. Rev. Genet. *20*, 536–548. https://doi.org/10.1038/s41576-019-0130-6.
12. Raj, A., and van Oudenaarden, A. (2008). Nature, nurture, or chance: stochastic gene expression and its consequences. Cell *135*, 216–226. https://doi.org/10.1016/j.cell.2008.09.050.
13. Kiviet, D.J., Nghe, P., Walker, N., Boulineau, S., Sunderlikova, V., and Tans, S.J. (2014). Stochasticity of metabolism and growth at the single-cell level. Nature *514*, 376–379. https://doi.org/10.1038/nature13582.
14. Taheri-araghi, S., Bradde, S., Sauls, J.T., Hill, N.S., Levin, P.A., Paulsson, J., Vergassola, M., and Jun, S. (2015). Cell-Size Control and Homeostasis in Bacteria. Curr. Biol. *25*, 385–391.
15. Nikolic, N., Schreiber, F., Dal Co, A., Kiviet, D.J., Bergmiller, T., Littmann, S., Kuypers, M.M.M., and Ackermann, M. (2017). Cell-to-cell variation and specialization in sugar metabolism in clonal bacterial populations. PLoS Genet. *13*, e1007122. https://doi.org/10.1371/JOURNAL.PGEN.1007122.
16. Vasdekis, A.E., and Singh, A. (2021). Microbial metabolic noise. WIREs Mech. Dis. *13*, e1512. https://doi.org/10.1002/wsbm.1512.
17. Fuentes, D.A.F., Manfredi, P., Jenal, U., and Zampieri, M. (2021). Pareto optimality between growth-rate and lag-time couples metabolic noise to phenotypic heterogeneity in Escherichia coli. Nat. Commun. *121*, 3204–3212. https://doi.org/10.1038/s41467-021-23522-0.
18. Erickson, D.W., Schink, S.J., Patsalo, V., Williamson, J.R., Gerland, U., and Hwa, T. (2017). A global resource allocation strategy governs growth transition kinetics of Escherichia coli. Nature *551*, 119–123. https://doi.org/10.1038/nature24299.
19. You, C., Okano, H., Hui, S., Zhang, Z., Kim, M., Gunderson, C.W., Wang, Y.-P., Lenz, P., Yan, D., and Hwa, T. (2013). Coordination of bacterial proteome with metabolism by cyclic AMP signalling. Nature *500*, 301–306. https://doi.org/10.1038/nature12446.
20. Gerosa, L., Kochanowski, K., Heinemann, M., and Sauer, U. (2013). Dissecting specific and global transcriptional regulation of bacterial gene expression. Mol. Syst. Biol. *9*, 658. https://doi.org/10.1038/msb.2013.14.
21. Boulineau, S., Tostevin, F., Kiviet, D.J., ten Wolde, P.R., Nghe, P., and Tans, S.J. (2013). Single-cell dynamics reveals sustained growth during diauxic shifts. PLoS One *8*, e61686. https://doi.org/10.1371/journal.pone.0061686.

22. Pedraza, J.M., and van Oudenaarden, A. (2005). Noise propagation in gene networks. Science *307*, 1965–1969. https://doi.org/10.1126/science.1109090.

23. Chalancon, G., Ravarani, C.N.J., Balaji, S., Martinez-Arias, A., Aravind, L., Jothi, R., and Babu, M.M. (2012). Interplay between gene expression noise and regulatory network architecture. Trends Genet. *28*, 221–232. https://doi.org/10.1016/j.tig.2012.01.006.

24. Dunlop, M.J., Cox, R.S., Levine, J.H., Murray, R.M., and Elowitz, M.B. (2008). Regulatory activity revealed by dynamic correlations in gene expression noise. Nat. Genet. *40*, 1493–1498. https://doi.org/10.1038/ng.281.

25. Kleijn, I.T., Krah, L.H.J., and Hermsen, R. (2018). Noise propagation in an integrated model of bacterial gene expression and growth. PLoS Comput. Biol. *14*, e1006386. https://doi.org/10.1371/journal.pcbi.1006386.

26. Rosenfeld, N., Young, J.W., Alon, U., Swain, P.S., and Elowitz, M.B. (2005). Gene Regulation at the Single-Cell Level. Science *307*, 1962–1965.

27. Stawsky, A., Vashistha, H., Salman, H., and Brenner, N. (2022). Multiple timescales in bacterial growth homeostasis. iScience *25*, 103678. https://doi.org/10.1016/j.isci.2021.103678.

28. el-Mansi, E.M., and Holms, W.H. (1989). Control of Carbon Flux to Acetate Excretion During Growth of Escherichia coli in Batch and Continuous Cultures. J. Gen. Microbiol. *135*, 2875–2883.

29. Cano, M., Holland, S.C., Artier, J., Burnap, R.L., Ghirardi, M., Morgan, J.A., and Yu, J. (2018). Glycogen Synthesis and Metabolite Overflow Contribute to Energy Balancing in Cyanobacteria. Cell Rep. *23*, 667–672. https://doi.org/10.1016/j.celrep.2018.03.083.

30. Kochanowski, K., Gerosa, L., Brunner, S.F., Christodoulou, D., Nikolaev, Y.V., and Sauer, U. (2017). Few regulatory metabolites coordinate expression of central metabolic genes in Escherichia coli. Mol. Syst. Biol. *13*, 903. https://doi.org/10.15252/msb.20167402.

31. Gerosa, L., Haverkorn Van Rijsewijk, B.R.B., Christodoulou, D., Kochanowski, K., Schmidt, T.S.B., Noor, E., and Sauer, U. (2015). Pseudo-transition Analysis Identifies the Key Regulators of Dynamic Metabolic Adaptations from Steady-State Data. Cell Syst. *1*, 270–282. https://doi.org/10.1016/J.CELS.2015.09.008.

32. Kaplan, S., Bren, A., Dekel, E., and Alon, U. (2008). The incoherent feed-forward loop can generate non-monotonic input functions for genes. Mol. Syst. Biol. *4*, 203. https://doi.org/10.1038/MSB.2008.43.

33. Lawson, C.L., Swigon, D., Murakami, K.S., Darst, S.A., Berman, H.M., and Ebright, R.H. (2004). Catabolite activator protein: DNA binding and transcription activation. Curr. Opin. Struct. Biol. *14*, 10–20. https://doi.org/10.1016/j.sbi.2004.01.012.

34. Hudson, J.M., and Fried, M.G. (1990). Co-operative interactions between the catabolite gene activator protein and the lac repressor at the lactose promoter. J. Mol. Biol. *214*, 381–396. https://doi.org/10.1016/0022-2836(90)90188-R.

35. Bren, A., Park, J.O., Towbin, B.D., Dekel, E., Rabinowitz, J.D., and Alon, U. (2016). Glucose becomes one of the worst carbon sources for E.coli on poor nitrogen sources due to suboptimal levels of cAMP. Sci. Rep. *6*, 24834. https://doi.org/10.1038/srep24834.

36. Thomas, P., Terradot, G., Danos, V., and Weiße, A.Y. (2018). Sources, propagation and consequences of stochasticity in cellular growth. Nat. Commun. *9*, 4528. https://doi.org/10.1038/s41467-018-06912-9.

37. Dekel, E., and Alon, U. (2005). Optimality and evolutionary tuning of the expression level of a protein. Nature *436*, 588–592. https://doi.org/10.1038/nature03842.

38. Bar-Even, A., Paulsson, J., Maheshri, N., Carmi, M., O'Shea, E.K., Pilpel, Y., and Barkai, N. (2006). Noise in protein expression scales with natural protein abundance. Nat. Genet. *38*, 636–643. https://doi.org/10.1038/ng1807.

39. Wolf, L., Silander, O.K., and van Nimwegen, E. (2015). Expression noise facilitates the evolution of gene regulation. Elife *4*, e05856. https://doi.org/10.7554/eLife.05856.

40. Vasdekis, A.E., Alanazi, H., Silverman, A.M., Williams, C.J., Canul, A.J., Cliff, J.B., Dohnalkova, A.C., and Stephanopoulos, G. (2019). Eliciting the impacts of cellular noise on metabolic trade-offs by quantitative mass imaging. Nat. Commun. *101*, 848. https://doi.org/10.1038/s41467-019-08717-w.

41. Hermsen, R., Okano, H., You, C., Werner, N., and Hwa, T. (2015). A growth-rate composition formula for the growth of E.coli on co-utilized carbon substrates. Mol. Syst. Biol. *11*, 801. https://doi.org/10.15252/msb.20145537.

42. De Martino, D., Capuani, F., and De Martino, A. (2016). Growth against entropy in bacterial metabolism: the phenotypic trade-off behind empirical growth rate distributions in E. coli. Phys. Biol. *13*, 036005. https://doi.org/10.1088/1478-3975/13/3/036005.

43. Susman, L., Kohram, M., Vashistha, H., Nechleba, J.T., Salman, H., and Brenner, N. (2018). Individuality and slow dynamics in bacterial growth homeostasis. Proc. Natl. Acad. Sci. USA *115*, E5679–E5687. https://doi.org/10.1073/pnas.1615526115.

44. Singh, A., Razooky, B.S., Dar, R.D., and Weinberger, L.S. (2012). Dynamics of protein noise can distinguish between alternate sources of gene-expression variability. Mol. Syst. Biol. *8*, 607. https://doi.org/10.1038/msb.2012.38.

45. Lin, J., and Amir, A. (2020). From single-cell variability to population growth. Phys. Rev. E *101*, 012401. https://doi.org/10.1103/PhysRevE.101.012401.

46. Shahrezaei, V., and Marguerat, S. (2015). Connecting growth with gene expression: Of noise and numbers. Curr. Opin. Microbiol. *25*, 127–135. https://doi.org/10.1016/j.mib.2015.05.012.

47. De Martino, D., MC Andersson, A., Bergmiller, T., Guet, C.C., and Tkačik, G. (2018). Statistical mechanics for metabolic networks during steady state growth. Nat. Commun. *9*, 2988. https://doi.org/10.1038/s41467-018-05417-9.

48. Smith, M., Ghusinga, K.R., and Singh, A. (2019). Comparison of feedback strategies for noise suppression in protein level. In American Control Conference, pp. 1513–1518, IEEE. https://doi.org/10.23919/ACC.2019.8815616.

49. Hermsen, R., Erickson, D.W., and Hwa, T. (2011). Speed, sensitivity, and bistability in auto-activating signaling circuits. PLoS Comput. Biol. *7*, e1002265. https://doi.org/10.1371/journal.pcbi.1002265.

50. Kittisopikul, M., and Süel, G.M. (2010). Biological role of noise encoded in a genetic network motif. Proc. Natl. Acad. Sci. USA *107*, 13300–13305. https://doi.org/10.1073/PNAS.1003975107.

51. Bruggeman, F.J., and Teusink, B. (2018). Living with noise: on the propagation of noise from molecules to phenotype and fitness. Curr. Opin. Struct. Biol. *1*, 7. https://doi.org/10.1016/j.coisb.2018.02.010.

52. Hooshangi, S., and Weiss, R. (2006). The effect of negative feedback on noise propagation in transcriptional gene networks. Chaos *16*, 026108. https://doi.org/10.1063/1.2208927.

53. Maheshri, N., and O'Shea, E.K. (2007). Living with Noisy Genes: How Cells Function Reliably with Inherent Variability in Gene Expression. Annu. Rev. Biophys. Biomol. Struct. *36*, 413–434. https://doi.org/10.1146/annurev.biophys.36.040306.132705.

54. Tonn, M.K., Thomas, P., Barahona, M., and Oyarzún, D.A. (2019). Stochastic modelling reveals mechanisms of metabolic heterogeneity. Commun. Biol. *2*, 108–109. https://doi.org/10.1038/s42003-019-0347-0.

55. Wehrens, M., Büke, F., Nghe, P., and Tans, S.J. (2018). Stochasticity in cellular metabolism and growth: Approaches and consequences. Curr. Opin. Struct. Biol. *8*, 131–136. https://doi.org/10.1016/J.COISB.2018.02.006.

56. Büke, F., Grilli, J., Cosentino Lagomarsino, M., Bokinsky, G., and Tans, S.J. (2022). ppGpp is a bacterial cell size regulator. Curr. Biol. *32*, 1–8. https://doi.org/10.1016/j.cub.2021.12.033.

57. Steinchen, W., Zegarra, V., and Bange, G. (2020). (p)ppGpp: Magic Modulators of Bacterial Physiology and Metabolism. Front. Microbiol. *0*, 2072. https://doi.org/10.3389/FMICB.2020.02072.

58. Zhu, M., and Dai, X. (2019). Growth suppression by altered (p)ppGpp levels results from non-optimal resource allocation in Escherichia coli. Nucleic Acids Res. *47*, 4684–4693. https://doi.org/10.1093/NAR/GKZ211.

59. Lin, W.H., and Jacobs-Wagner, C. (2022). Connecting single-cell ATP dynamics to overflow metabolism, cell growth, and the cell cycle in Escherichia coli. Curr. Biol. *32*, 3911–3924.e4. https://doi.org/10.1016/j.cub.2022.07.035.

60. Young, J.W., Locke, J.C.W., Altinok, A., Rosenfeld, N., Bacarian, T., Swain, P.S., Mjolsness, E., and Elowitz, M.B. (2011). Measuring single-cell gene expression dynamics in bacteria using fluorescence time-lapse microscopy. Nat. Protoc. *7*, 80–88. https://doi.org/10.1038/nprot.2011.432.

61. Walker, N., Nghe, P., and Tans, S.J. (2016). Generation and filtering of gene expression noise by the bacterial cell cycle. BMC Biol. *14*, 11. https://doi.org/10.1186/s12915-016-0231-z.

STAR★METHODS

KEY RESOURCES TABLE

REAGENT or RESOURCE	SOURCE	IDENTIFIER
Bacterial and virus strains		
Wild type MG1655, also known as strain bBT12 and CGSC number 8003. Known mutations: λ−, Δfnr-267, rph-1. (No resistance modules.)	Alon lab[5]	ASC838; bBT12; CGSC#8003
cyaA, cpda null mutant. Also known as strain bBT80. Based on ASC838. (No resistance modules.)	Alon lab[5]	ASC839; bBT80
Referred to as "WT" in the manuscript. Wild type strain, except for Δ(galk):nCRPr-mCerulean-kanR and Δ(intc):CRPr-mVenus-cmR. (Kanamycin and chloramphenicol resistant.)	This paper	ASC990
Referred to as cAMP-fixed in the manuscript. Strain based on ASC839 (ΔcyaA Δcpda), with inserted reporters Δ(galk):s70-mCerulean-kanR and Δ(intc):rcrp-Venus-cmR. (Kanamycin and chloramphenicol resistant.)	This paper	ASC1004
Chemicals, peptides, and recombinant proteins		
Cyclic adenosine monophosphate (cAMP)	Sigma Aldrich	Cat#A6885
Lactose	Merck	N/A
Tween 20	Sigma Aldrich	N/A
Uracil	Merck	N/A
Software and algorithms		
Metamorph 7.8.0.0	Molecular Devices	https://www.moleculardevices.com
MATLAB 9.1.0.441655 (R2016b)	MathWorks	https://www.mathworks.com/products/matlab.html
Custom MATLAB segmentation and MATLAB & Mathematica analysis scripts	Tans lab	https://doi.org/10.5281/zenodo.8335363
Mathematica 13	Wolfram	https://www.wolfram.com/mathematica

RESOURCE AVAILABILITY

Lead contact

Further information and requests for resources and reagents should be directed to and will be fulfilled by the lead contact, Sander J. Tans (tans@amolf.nl).

Materials availability

Bacterial strains generated in this study are available upon request with the lead contact.

Data and code availability

- Single cell time lapse and lineage data are available on request with the lead contact.
- All original code has been deposited at Zenodo and is publicly available as of the date of publication. DOIs are listed in the key resources table.
- Any additional information required to reanalyze the data reported in this paper is available from the lead contact upon request.

EXPERIMENTAL MODEL AND SUBJECT DETAILS

Microbe strains

All strains used were based on wild type strain MG1655 (CGSC 8003, bBT12). The CRPr and nCRPr promoters were based on the lac operon promoter, with respectively the lacI binding site or both lacI and CRP binding site scrambled.[5] To obtain the C-sector reporter (CRPr) and constitutive reporter (nCRPr), we fused these promoters to mCerulean and mVenus sequences respectively. The reporters where then inserted into the chromosomes of the bBT12 strain and a cyaA cpda null mutant strain constructed earlier (bBT80), using a lambda red protocol.[5] See key resource table for strain details and Figure S1A for promoter sequences.

Bulk measurements

To determine growth rates of the cyaA cpdA null mutant strain (strain ASC1004, also referred to as cAMP-fixed) at different cAMP concentrations, this strain was inoculated from a freeze mix stock (kept at −80 C) into TY medium, and grown for several hours until exponential growth was achieved. The culture was then diluted (>1000x) into M9 minimal medium supplemented with 0.2 mM uracil, 0.1% lactose, 800 μM cAMP and grown O/N to allow cells to adjust to the lactose medium. Subsequently, the culture was inoculated into separate wells each containing M9 medium with a different final concentration of cAMP (3.1M, 8.7M, 25.8 μM, 82.7 μM, 272.1 μM, 903.1 μM, 3004.3 μM and 10001.3 μM cAMP, with identical supplements, on a 96 well plate). The samples were then grown for several hours in a Wallac 1420 VICTOR3 Multilabel Counter (PerkinElmer) to record OD values over time in triplicate. Everything was conducted at 37 C.

Single cell experiments

Micro-colonies of cells were grown on gel pads, imaged under a microscope, and analyzed by computer as described earlier.[13,55] Briefly, polyacrylamide gel pads (approx. 5 mm × 5 mm x 1 mm in size) were pre-soaked in M9 minimal medium supplemented with lactose (0.01% g/mL), uracil (0.2 mM), Tween 20 (0.001%) and the desired concentration of cAMP (Sigma Aldrich) if applicable. Pads were placed in a sealed glass chamber created by a microscope slide and a 2nd glass cavity slide, covered by a glass coverslip. Cells were pre-grown overnight in the same medium, and 1 μL of exponentially growing culture (OD 0.005) was then inoculated on the gel pad at the start of the experiment. Everything was done at 37°C, and the glass chamber with pad and cells was then placed in a customized scaffold, and imaged under a microscope with a customized incubation chamber at 37°C. For the WT, cAMP-fixed^{low}, cAMP-fixed* and cAMP-fixed^{high} conditions, we respectively processed time series data from 6, 2, 4 and 2 micro-colonies.

METHOD DETAILS

Microscopy

We used a Nikon, TE2000 microscope, equipped with 100× oil immersion objective (Nikon, Plan Fluor NA 1.3), cooled CMOS camera (Hamamatsu, Orca Flash4.0), xenon lamp with liquid light guide (Sutter, Lambda LS), GFP, mCherry, CFP and YFP filter set (Chroma, 41017, 49008, 49001 and 49003), computer controlled shutters (Sutter, Lambda 10–3 with SmartShutter), automated stage (Märzhäuser, SCAN IM 120 x 100) and an incubation chamber (Solent) allowing precise 37°C temperature control. An additional 1.5X lens was used, resulting in images with pixel size of 0.0438 μm. The microscope was controlled by MetaMorph software, which allowed us to automatically take pictures at set intervals. Image acquisition intervals were adjusted to doubling times to obtain multiple fluorescent images per cell cycle; phase contrast images were taken every 60–90 s, CFP and YFP fluorescent images (150–200 ms exposure time) were taken at intervals ranging from 13.5 to 26 min.

Image analysis

Series of phase contrast images were analyzed with the MATLAB (Mathworks) program Schnitzcells,[60] extended with custom scripts written by Daan Kiviet, Philippe Nghe, and Noreen Walker.[13,61] Cells were segmented and tracked to follow cells and lineages through time in line with Kiviet et al.[13] For each frame, cell lengths were determined by fitting a 3rd (or, in some cases 5th) order polynomial to the curved segmentation regions. Cells were assumed to have a constant width. Growth rates (dbl/hr) were determined by fitting an exponential function to the cell lengths over multiple frames (5–9). To determine the production rate per volume, first the sum of the fluorescence signal (a.u.) over all pixels that make up a cell was calculated. If on frame n also a fluorescence image was taken, we then calculated the slope of a linear fit through three points $n - I$, n, and $n + I$ (where I is the frame interval at which fluorescence pictures are taken), the resulting number is divided by the total number of pixels of the cell in frame n to obtain the production rate. Concentrations were determined by dividing the sum of the fluorescence signal by the total number of pixels in a cell. To determine scatterplots and correlations, only frames where fluorescence images were taken are considered.

Mathematical model

As mentioned, our model consists of stochastic differential equations, and includes variables representing protein production rates (π), protein concentrations (φ), metabolism (M), growth rate (λ), and Ornstein-Uhlenbeck noise sources N. Parameters include noise transfer coefficients T that couple equations for $d\pi/dt$, $d M/dt$, and $d \lambda/dt$; concentrations are determined by $d\varphi/dt = \pi - \varphi\lambda$. This model is solved analytically to predict cross-correlations between the quantities. See Data S1 for an extensive description of the

model, procedures to fit the model to experimental data, a statistical null model for the cross-correlations, and a toy model that describes the mean behavior of π, φ, and λ for CRPr and nCRPr in different conditions as observed in Figure 3.

QUANTIFICATION AND STATISTICAL ANALYSIS

Statistical details of experiments are listed in figure captions. In Figure 1, data from $n = 1671$ (WT) and $n = 1580$ (cAMP-fixed*) cells are shown. To determine the statistical significance of the difference between the φ_{CRPr}-λ slopes in WT and cAMP-fixed*, a Student's t-test was performed, after confirmation that the test's assumptions were valid (based on $n = 6$ and $n = 4$ microcolonies). To determine the statistical significance of the difference between the WT and cAMP-fixed* φ_{nCRPr}-λ slopes, a Welch's t-test was performed, as the variances were unequal (based on $n = 6$ and $n = 4$ microcolonies). Cross-correlations in Figure 2 are based on $n = 113, 63, 110, 953, 729, 1667$ cells (WT) and $n = 1568, 1626, 1500, 837$ cells (cAMP-fixed*), from respectively 6 (WT) and 4 (cAMP-fixed*) microcolony measurements. Data presented in Figure 3 are based on $n = 1165, 623$ (cAMP-fixed$^{\mathrm{low}}$), $n = 1568, 1626, 1500$ (cAMP-fixed*) and $n = 1437, 837$ (cAMP-fixed$^{\mathrm{high}}$) cells from respectively 2, 3 and 2 microcolonies. See below for further details of the cross-correlation analysis.

Cross-correlation analysis

In general, the cross-covariance χ and cross-correlation R between two signals in discrete time are defined as:

$$\chi_{f,g}(\tau) = \frac{1}{N - |\tau| - 1} \sum_{n=0}^{N-|\tau|-1} \hat{f}(n)\hat{g}(n + \tau), \text{and} \quad R_{f,g}(\tau) = \frac{\chi_{f,g}(\tau)}{\sqrt{\chi_{f,f}(0)\chi_{g,g}(0)}},$$

where hats indicate mean-subtracted signals.

Cells that are born earlier in the experiments appear in more lineages. When calculating cross-correlations along lineages, we must therefore be careful to not count such cells repeatedly. Therefore, we introduce for each data point a weight representing in the number of branches it occurs in. The result is a composite cross-correlation with contributions of points from multiple branches i. Lastly, we also introduce time-average-subtracted variables. We therefore define a composite cross-covariance and cross-correlation:

$$S_{f,g}(\tau) := \frac{1}{W_{\mathrm{total},\tau}} \sum_i \frac{1}{N_i - |\tau| - 1} \sum_{n=0}^{N_i-|\tau|-1} w_{n,i,\tau} \hat{f}_i(n)\hat{g}_i(n + \tau)$$

$$\mathcal{R}_{f,g}(\tau) = \frac{S_{f,g}(\tau)}{\sqrt{S_{f,f}(0)S_{g,g}(0)}}$$

$$\hat{f}_i(n) = f_i(n) - \langle f_i \rangle_n$$

$$w_{n,i,\tau} = 1/K_{n,i,\tau},$$

$$W_{\mathrm{total},\tau} = \sum_{n,i} w_{n,i,\tau}.$$

Here, the summations run over all branches i and time points n. Weights are indicated with w, where $K_{n,i,\tau}$ is the frequency with which a specific point pair $\hat{f}_i(n)\hat{g}_i(n + \tau)$ was used. Throughout the manuscript we refer to the composite cross-correlation $\mathcal{R}$ as the cross-correlation R. The mean-subtracted signal $\hat{f}_i(n)$ is now recalculated in each branch, for each time point, to compensate for a changing overall average during the experiment.

To confirm that the measured cross-correlations correspond to biological signals inside the cells, we performed a permutation analysis on the time-series data. We kept the temporal information of the data, but randomized at each time point the growth rate and expression data for all the cells in the colony. Any biological correlations between variables should therewith be removed. Repeating this randomization 50 times, and each time re-calculating cross-correlations, indeed gives a band of cross-correlations around zero, allowing us to infer what kind of signals could still be explained purely by technical noise (see for example Figures S3J–S3M). Any part of the originally measured cross-correlations that fall outside this band can then be concluded to stem from a real biological signal .

To create Figures 2 and 3 of the main text, the cross-correlations calculated per microcolony were averaged. Here, we explain how we averaged for each growth-condition the multiple (independent) experiments (each microcolony being an experiment), and how we calculated error bars. In short, we determine the consistency of a microcolony by dividing the colony in multiple roughly equal parts

and calculate for each delay time the (cross)-correlations of growth rate and protein production/concentration over these parts. To determine an average using multiple microcolonies grown at the same condition, microcolonies with a higher internal variance are weighted less (as a high variance is likely the result of non-uniform growth conditions across the agar plate, or it could hint at other biological processes like filamentation that would disrupt the measurement).

To be more precise, we write N for the number of experiments and n_i for the number of subgroups within experiment i. To estimate error bars, we use a statistical model with random effects. We assumed that a measurement y_{ij} based on part $j \in \{1, \ldots, n_i\}$ of experiment $i \in \{1, .., N\}$ is determined by the average of interest, μ, plus two noise sources: within-experiment noise ξ_{ij}, and between-experiment noise η_i:

$$y_{ij} = \mu + \eta_i + \xi_{ij}.$$

Here, the random variable η_i represents the systematic off-set of the mean in experiment i, and the random variable ξ_{ij} represents noise in the measurements specific to part j of group i. Both η_i and ξ_{ij} are assumed to be sampled independently from their respective probability distributions, with means zero, *i.e.*, $[\eta_i] = E[\xi_{ij}] = 0$.

It follows that $E[y_{ij}] = \mu$.

Furthermore, we write $\mathrm{Var}[\xi_{ij}] = \sigma_i^2$ for the variance introduced by the random differences between parts within experiment i (σ_i^2 might differ between experiments), and $\mathrm{Var}[\eta_i] = \sigma^2$ for the variance introduced by systematic differences between experiments.

The mean over all measurements is written as $\bar{y}$, and equals, per definition of the mean:

$$\bar{y} = \frac{\sum_{i=1}^{N} \sum_{j=1}^{n_i} y_{ij}}{\sum_{i=1}^{N} n_i}.$$

With the notation above, the variance of the mean of the measurements can be written as:

$$\mathrm{Var}[\bar{y}] := \frac{\mathrm{Var}\left[\sum_{i=1}^{N} \sum_{j=1}^{n_i} \mu + \eta_i + \xi_{ij}\right]}{\left(\sum_{i=1}^{N} n_i\right)^2}$$

$$= \frac{1}{\left(\sum_{i=1}^{N} n_i\right)^2} \mathrm{Var}\left[\sum_{i=1}^{N} n_i \eta_i + \sum_{i=1}^{N} \sum_{j=1}^{n_i} \xi_{ij}\right]$$

$$= \frac{1}{\left(\sum_{i=1}^{N} n_i\right)^2} \left(\sum_{i=1}^{N} n_i^2 \mathrm{Var}[\eta_i] + \sum_{i=1}^{N} n_i \mathrm{Var}[\xi_{ij}]\right)$$

$$= \frac{\sigma^2 \sum_{i=1}^{N} n_i^2 + \sum_{i=1}^{N} n_i \sigma_i^2}{\left(\sum_{i=1}^{N} n_i\right)^2}$$

Note that $\sqrt{\mathrm{Var}[\bar{y}]}$ is the standard deviation of the mean (standard error). This standard error $\sqrt{\mathrm{Var}[\bar{y}]}$ can estimated by using the above equation and estimating σ and σ_i from the experiments. To estimate σ_i, we calculated the standard deviation s_i among the measurements of parts j in experiment i; to estimate σ we calculated the standard deviation among the means calculated per experiment. The error bars in Figures 2B and and 3D and E represent the resulting standard errors.

In practice, n_i had the same value in all our experiments ($n_i = 4$ for all i).

Writing $n_i = n$, the equation for the standard error reduces to

$$\mathrm{Var}[\bar{y}] = \frac{\sigma^2}{N} + \frac{\sum_{i=1}^{N} \sigma_i^2 / N}{nN}.$$

This shows that the variance of the observed mean $\bar{y}$ has two contributions: the variance introduced by systematic differences between experiments, which decreases with the number of experiments, and the variance introduced by differences between parts of the same experiment, which decreases with the number of observations n.

To best estimate the average, μ, we again use knowledge of within-experiment variances to calculate a weight factor for each microcolony. Let $y_i(t)$ be the measured mean value of an observable in experiment i at time t, with within-experiments error $s_i(t)$. Then we estimate the weighted average as:

$$\langle y(t)\rangle = \frac{\sum_{i=1}^{N} s_i^{-2}(t) y_i(t)}{\sum_{k=1}^{N} s_k^{-2}(t)} = : \frac{\sum_{k=1}^{N} w_i(t) y_i(t)}{W(t)}.$$

Here, $w_i(t) = s_i^{-2}(t)$ and $W(t) = \sum_{k=1}^{N} w_k(t)$. That is, more precise measurements (*i.e.*, those with smaller within-experiment error s_i) obtain a higher weight.

The within experiment variances s_i^2 are estimated by dividing each microcolony into four lineages (*i.e.*, $n_i = 4$ for all experiments); from the moment there were four cells in the microcolony, we followed each of their lineages separately, and calculated and compared cross-correlations along each lineage.

Cell Reports, Volume *42*

Supplemental information

The interplay between metabolic stochasticity and cAMP-CRP regulation in single *E. coli* cells

Martijn Wehrens, Laurens H.J. Krah, Benjamin D. Towbin, Rutger Hermsen, and Sander J. Tans

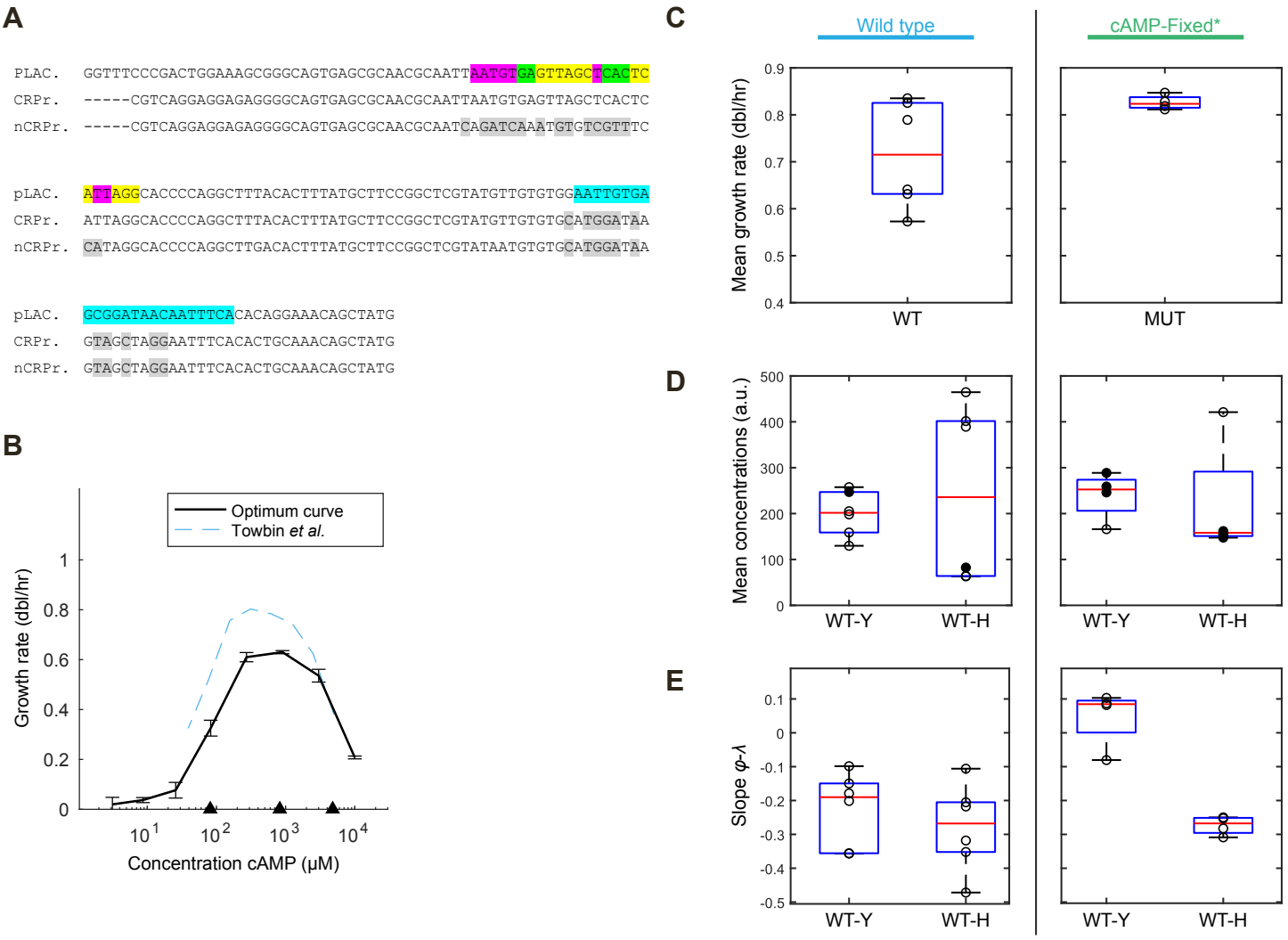

Figure S1. Reporter constructs, bulk growth rates and average experimental values measured in different colonies, related to Figure 1.
(A) Overview of promoter sequences used in this manuscript. The top row indicates the original LacZ upstream region including start codon ATG (NCBI; gene ID 945006, NC 000913.3), whilst the 2nd and 3rd row give the sequence of the engineered CRPr and nCRPr promoters. Colour indicates CRP binding sites according to Hudson and Fried [S1] (yellow), Lawson et al. [S2] (green) or both (purple), and the LacI binding site (blue) according to Hudson and Fried [S1]. In grey, changes in the engineered promoters are indicated. **(B)** Exponential phase growth rates of the cyaA cpdA null mutant (cAMP-fixed cells) at different concentrations of cAMP as measured in a plate reader. Black triangles refer to the low, optimal and high cAMP concentrations respectively. The growth rate was determined as an exponential fit over a manually selected part of the bacterial density curve. Additionally, this figure shows data from a similar experiment performed by Towbin et al. [S3]. **(C)** Average growth rate per colony, showing a large variance in growth-rate measurements. Difference between the mean growth rates of WT and cAMP-fixed* cells is not significant (p = 0.063, Welch's t-test). **(D)** Average fluorescence per colony. Filled circles are values measured with a standardized microscope setting (and thus only those absolute values can be compared). **(E)** Regression slope between φ and λ for the wild type and cAMP-fixed* cells (MUT in the figure). Slopes for the Y reporter differ significantly between wild type and mutant cAMP-fixed* cells (p = 0.0031, two-sample t-test), but not for the H reporter (p = 0.93, Welch's t-test). Note that to calculate these regression slopes only relative fluctuations are relevant, so that only relative fluorescence signals are relevant. Y: C-sector reporter, H: constitutive reporter.

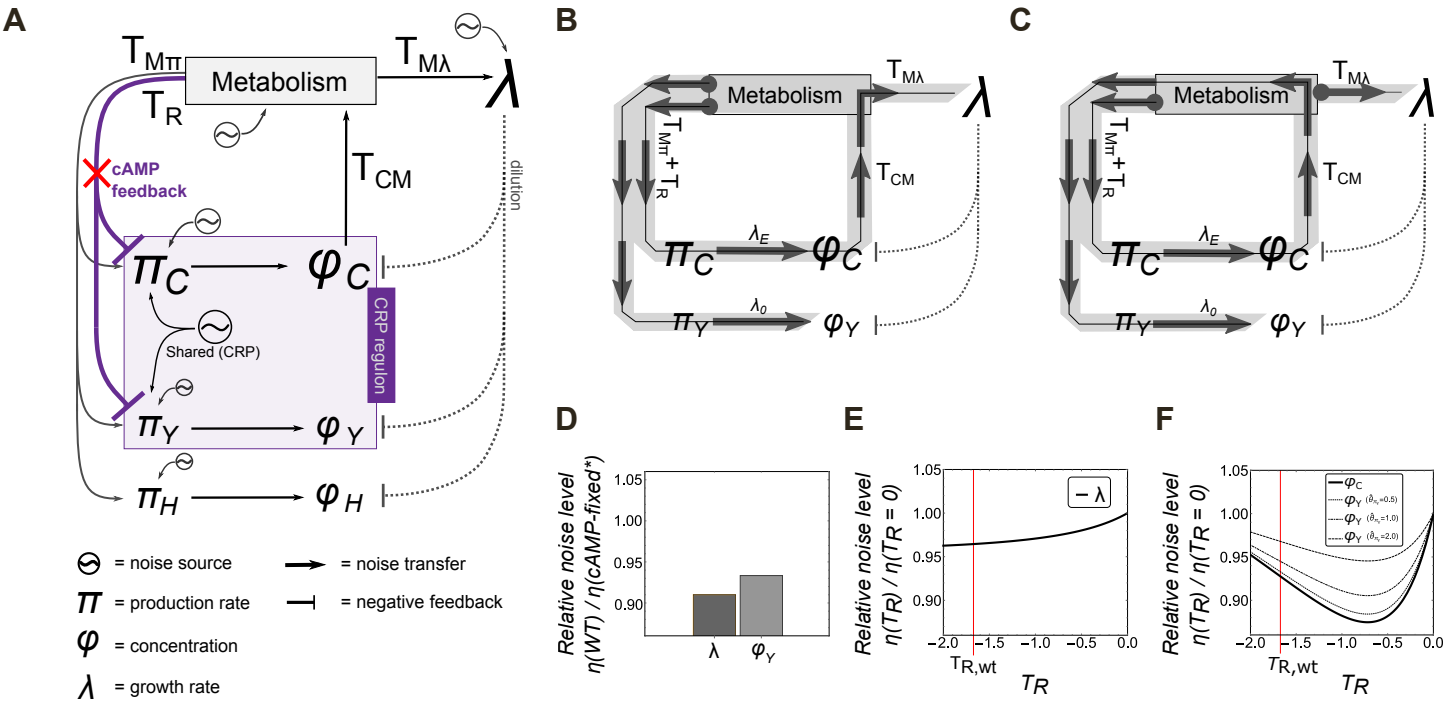

Figure S2. Mathematical model pinpoints dynamical role of regulation and predicts noise decrease due to feedback, related to Figure 2.
(A) Diagram of proposed mathematical model reflecting the biological wiring of a bacterial cell. The model includes the C reporter (*Y*) and constitutive reporter (*H*). Intrinsic noise in the protein production rates, metabolism and the growth rate is modeled as independent Ornstein-Uhlenbeck noise sources. An additional shared noise source (here called N_s) acts on both π_C and π_Y. N_s represents noise in the sensory mechanism (for example fluctuations of the CRP-concentration). The transfer from Metabolism (*M*) to protein production is the sum of general transfer ($T_{M\pi}$) and regulatory transfer (T_R), which only acts on the C-sector and its reporter, *Y*. **(B,C)** Example analysis of two different noise routes from noise source N_M to φ_Y and λ (shown here is a only part of model). Thick gray arrows indicate the direction of a noise route and gray arrows with circles indicate the start of a route. In the left panel **(B)**, one path goes directly to φ_C and one path goes, via φ_C back to *M* and then transfers to λ. Transfer coefficients can be split up to represent the paths to φ_C and to λ separately as: $(T_{MC})(T_{MC}T_{CM}T_{M\lambda})$. In the right panel **(C)**, another example of an *M*-noise route: $(T_{MC}T_{CM}T_{MC})(T_{M\lambda})$. **(D)** Measured decrease in Coefficients of Variation (CV or η) for the growth rate (λ) and the CRP-sector reporter (ϕ_Y, or ϕ_{CRPr} in the main text). Data is the same as in Figure S3E. **(E)** Model prediction of the decrease in the CV of the growth rate, η_λ, for different feedback strengths. The vertical red line indicates the best-fit value for the WT condition. **(F)** Predicted decrease in CV for the CRP regulated sector (ϕ_C, thick solid line) and the corresponding CRP-regulated reporter θ_Y (ϕ_{CRPr} in the main text). A (relatively) larger amplitude of the noise-source intrinsic to the production rate of the CRP-regulated reporter, $\hat{\theta}_{\pi_Y}$, reduces the observability of the reduction in CV (dotted, dot-dashed and dashed lines for $\hat{\theta}_{\pi_Y}$ = 0.5, 1, and 2 respectively). Note additional parameters were fitted for these plots; all parameters are as in Table S2, except those varied in the figures (T_R and θ_{π_Y}). Although the relative reduction shows a quantitative similarity to the observed data, the model outcome does not match the observed absolute values for η_λ and η_{ϕ_Y}, possibly because of other noise sources not taken into account.

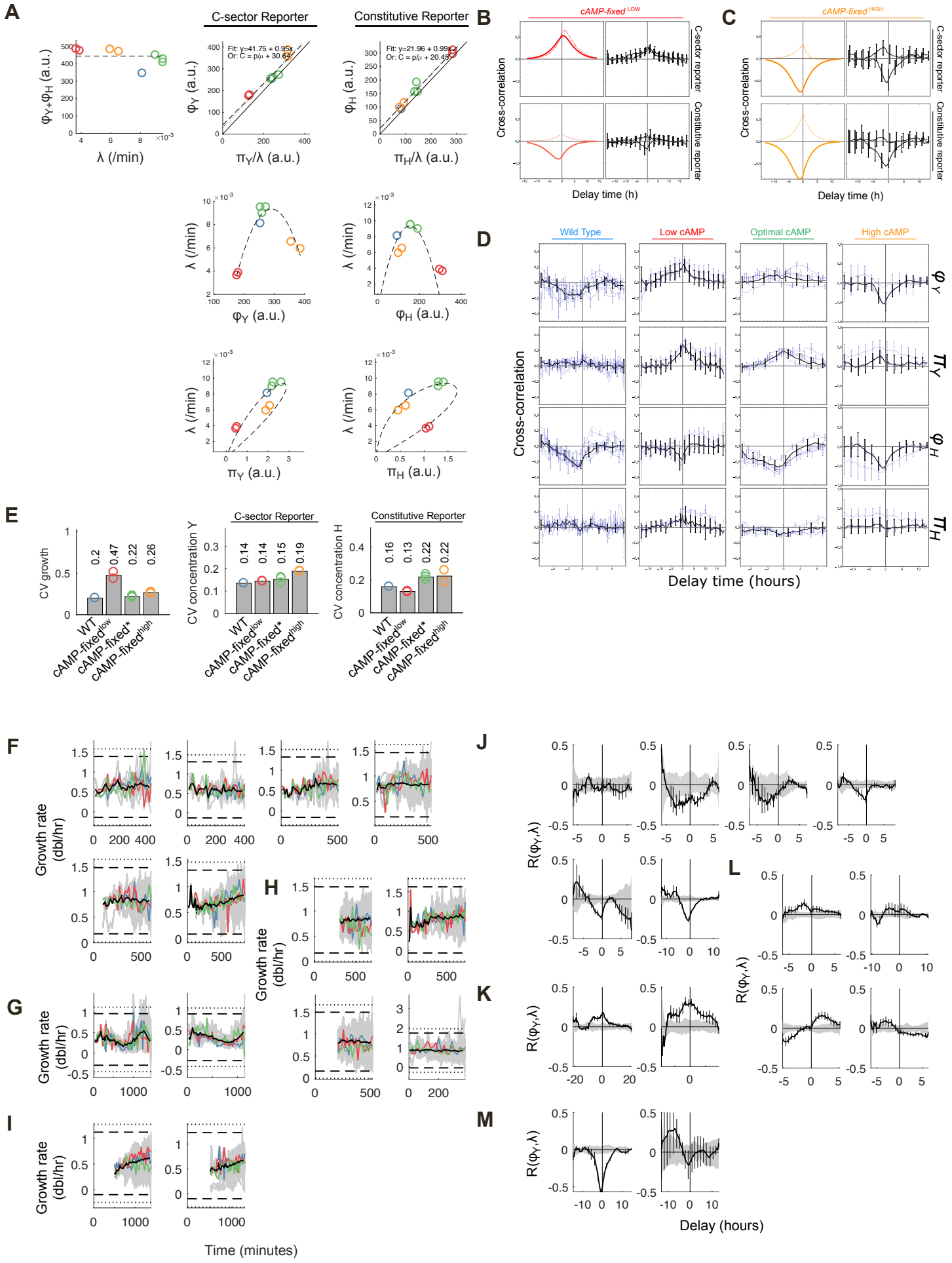
A
C-sector Reporter
Constitutive Reporter
B
cAMP-fixed LOW
C
cAMP-fixed HIGH
Cross-correlation
C-sector reporter
Constitutive reporter
Delay time (h)
D
Wild Type
Low cAMP
Optimal cAMP
High cAMP
Delay time (hours)
E
CV growth
CV concentration Y
CV concentration H
WT
cAMP-fixed low
cAMP-fixed*
cAMP-fixed high
F
G
H
I
Growth rate (dbl/hr)
Time (minutes)
J
K
L
M
R(φY,λ)
Delay (hours)

Figure S3. A toy model explains population behavior and cross-correlations from non-optimal conditions validate model, related to Figure 3.
(A) Our toy model fits the mean behavior of the reporters and the growth rate (see Data S1 for details). The sum of reporter concentrations is approximately constant in all conditions (top left panel). Furthermore, the steady state relationship $\varphi_Y=\pi_Y/\lambda$ (black straight line) holds closely for all conditions (2nd column, top panel). The best fit (dashed line), however, has a slight offset. In the 2nd column, 2nd row, the fitted parabolic relationship of φ_Y between the growth conditions. (See also S1B). In the 2nd column, bottom row, the relationship between π_Y and λ as calculated from the toy model. In the 3rd row, top panel, steady state relationship for the constitutive reporter. In the right column, the constitutive reporter concentrations and production rates for each condition fall on the curve calculated from the toy model (not fitted). Colour coding is as in other figures (blue: wild type, red: low cAMP mutant, green: medium cAMP mutant, orange: high cAMP mutant). Y: C-sector reporter, H: constitutive reporter. **(B-C)** Qualitative model prediction for the cross-correlations as measured in the cAMP-fixed cells using low-cAMP 80 μM, panel (B) and high-cAMP 5000 μM, panel (C) conditions, together with the measured cross-correlations. In panel (B), the transfer parameters from M to λ ($\hat{T}_{M\lambda}$) and from M to π ($T_{M\pi}$) have been increased by 0.3, and T_{CM} is slightly increased as well (scaled by 1.1; affecting $\hat{\theta}_M$, compared to the best-fit values from the cAMP-fixed* condition. In panel (C), same values as in (B) for $\hat{T}_{M\lambda}$ and $\hat{T}_{M\pi}$, but now T_{CM} is slightly negative (multiplied by -0.3). **(D)** All measured cross-correlations (thin blue lines) in independent replicates (independent colonies), together with their weighted averages (thick black lines), for all conditions. Y: C-sector reporter, H: constitutive reporter. **(E)** Coefficients of variation of the growth rate (left panel) and the concentrations of the C-sector reporter (middle panel) and the constitutive reporter (right panel) for the different conditions. Shown in the figure are only the experiments performed with similar microscope settings such that their absolute values were comparable. **(F-I)** Growth rates during the experiments. Each panel plots growth-rate data for a single colony; panels are grouped by growth condition. The gray lines show single lineage traces, the black lines the population average. Colored lines highlight example single lineage traces to illustrate single cell behavior. Dashed and dotted lines indicate 4σ and 5σ boundaries from the overall mean respectively. As before, the displayed conditions are wild type cells (F), cAMP-fixed* cells growing on 80 μM cAMP (G), cAMP-fixed cells growing on 800 μM cAMP (H) and mutant cells growing on 5000 μM cAMP (I). **(J-M)** Cross-correlations between the C-sector reporter, φ_Y, and λ, together with their null expectation (gray areas around 0, see STAR methods for details of the calculation). The black lines in this figures are the light-blue lines in top panels of Figure S3D. Error bars are calculated by dividing each microcolony into four parts and comparing statistics in each part. As before, the displayed plots are from independent microcolonies growing under the following conditions: wild type cells (J), cAMP-fixed cells growing on 80 μM cAMP (K), cAMP-fixed cells growing on 800 μM cAMP (L) and cAMP-fixed cells growing on 5000 μM cAMP (M).

Figures with data	Condition	# Colonies	# Cells	# Data Points
1C, 1E	WT	1	1671	5979
1D, 1F	Fixed-800	1	1580	4339
2B (left panels)	WT	6	113,63,110,953,729,1667	573,346,513,2420,1834,5979
2B (right panels)	Fixed-800	4	1568, 1626,1500,837	4339, 5202,4697,2664
3A, 3B, 3D	Fixed-80	2	1165, 623	4141,1985
3A, 3B	Fixed-800†	3	1568, 1626,1500	4339, 5202,4697
3A, 3B, 3E	Fixed-5000	2	1437,837	4229, 2086

Table S1. number of data points for all single cell experiments, related to Figure 1, 2 and 3.
Number of cells (as determined by custom Matlab scripts, see STAR Methods), number of colonies, and number of data points for all single cell experiments. (†Only a subset of data was used, as for those data sets microscopy conditions were equal, such that the values can be compared directly.)

Parameter	Confined to	Best Fit	95% confidence interval
θ_{π_C}	0	-	-
θ_S	1	-	-
T_{C_M}	1	-	-
T_F	[-2, 2] (WT); 0 (MUT)	**-1.67 (WT)**	[-2.28, -1.25]
T_R	[-1, 1]	**0.05**	[0.045, 0.54]
$\hat{T}_{M_\lambda}$	[-1, 1]	**-0.179**	[-0.22, -0.14]
$\hat{T}_{M_\pi}$	[0, 5]	**0.0**	[0, 0.74]
$\hat{\theta}_{\pi_y}$	[0, 5]	**1.14**	[1.06, 1.24]
$\hat{\theta}_{\pi_h}$	[0, 10]	**0.90**	[0.83, 0.97]
$\hat{\hat{\theta}}_M$	[0, 5]	**0.13**	[0.125, 0.143]
β_π	> 2	**2**	[1.8, 2.16]
β_μ	> 0.5	**0.78**	[0.75, 0.82]

Table S2. Best fit parameters of the model for the wild type and optimal mutant, related to Figure 2.
Best fit parameters including predefined parameter constraints and best-fit confidence ranges based on statistical analysis. Parameter T_R was set to 0 for cAMP-fixed* (MUT) cells. All other parameters were fitted using a minimization of the squared distance of 8 analytical curves (cross-correlations $\varphi - \lambda$ and $\pi - \lambda$ for both reporters. and for WT and $cAMP^{fixed*}$ cells) to the cross-correlation data (Fig. 2B from the main text). For the precise interpretation of $\hat{}$-parameters, see Data S1.

Supplemental References

[S1] Hudson, J.M., and Fried, M.G. (1990). Co-operative interactions between the catabolite gene activator protein and the lac repressor at the lactose promoter. J. Mol. Biol. 214, 381–396. 10.1016/0022-2836(90)90188-R.
[S2] Lawson, C.L., Swigon, D., Murakami, K.S., Darst, S.A., Berman, H.M., and Ebright, R.H. (2004). Catabolite activator protein: DNA binding and transcription activation. Curr. Opin. Struct. Biol. 14, 10–20. 10.1016/j.sbi.2004.01.012.
[S3] Towbin, B.D., Korem, Y., Bren, A., Doron, S., Sorek, R., and Alon, U. (2017). Optimality and sub-optimality in a bacterial growth law. Nat. Commun. 8, 14123. 10.1038/ncomms14123.